A Limited Area Model for Monsoon Prediction

S.S. Singh, S. S Vaidya and *E. N. Rajagopal*
Indian Institute of Tropical Meteorology, Pune-411005, India.
Received January 10, 1989

ABSTRACT

A six level regional primitive equation model has been formulated and tested for monsoon prediction. The model uses dynamic normal mode initialization scheme for obtaining initial balance. The physical processes included are: the large scale condensation, the Kuo type of cumulus convection, the surface friction, the sensible heat supply and evaporation over the sea. The actual smooth orography is included. The model has been integrated for 48 hrs using input of 7 July and 8 August 1979 when the domain of integration was dominated by an intense monsoon depression. In order to investigate the model simulation of formative stage of the depression, the model was also integrated using input of 4 July 1979.

Furthermore, the envelope orography has been constructed and included in the model for investigating its effects on the monsoon prediction. Results of the model forecast are presented and discussed.

I. INTRODUCTION

A regional five level primitive equation model in pressure coordinate with necessary physical processes was formulated and tested for monsoon prediction (Singh, 1985; Singh et al., 1988). The effect of orography was not included. Inclusion of orography excited the high frequency waves and contaminated the forecast fields particularly in the area of high orography. Since the sigma coordinate has been found to have advantage over the pressure coordinate, particularly in the treatment of orography, the development of a regional primitive equation model using sigma as vertical coordinate was taken up. The dynamical frame of the model is adopted from the Japan Meteorological Agency limited area forecast model (Electronic Computation Centre, JMA, 1983).

In this paper, we present the description of the model, the physical processes incorporated and finally the forecast results obtained for two cases of intense monsoon depression. Furthermore, the forecast results obtained with input of 4 July 1979 are presented and the impact of envelope orography has been discussed.

II. MODEL EQUATIONS

The model equations are in sigma coordinate on Mercator projection and are in flux from. The σ is defined as

$$\sigma = \frac{p - p_T}{p_s - p_T}. \tag{1}$$

p_s is surface pressure and p_T is the top of the model atmosphere which is 100 hPa in the present model. The $p_s - p_T$ is denoted as π. The pressure at any point on σ level is

related with π as follows

$$p = \sigma\pi + p_T.$$

The set of equations are as follows:

Momentum Equations

$$\frac{\partial}{\partial t}\left(\frac{\pi}{m^2}u\right) = -\frac{\partial}{\partial x}(u^* u) - \frac{\partial}{\partial y}(v^* u) - \frac{\partial}{\partial \sigma}\left(\frac{\pi}{m^2}\dot{\sigma}u\right)$$
$$+\frac{\pi}{m^2}v\left\{f - v\frac{\partial m}{\partial x} + u\frac{\partial m}{\partial y}\right\} - \frac{\pi}{m}\frac{\partial \varphi}{\partial x} - C_p\frac{\pi\theta}{m}\frac{\partial P^\kappa}{\partial x} + \frac{\pi}{m^2}F_u + \frac{g}{m^2}\left(\frac{\partial \vec{\tau}}{\partial \sigma}\right)_x, \tag{2}$$

$$\frac{\partial}{\partial t}\left(\frac{\pi}{m^2}v\right) = -\frac{\partial}{\partial x}(u^* v) - \frac{\partial}{\partial y}(v^* v) - \frac{\partial}{\partial \sigma}\left(\frac{\pi}{m^2}\dot{\sigma}v\right)$$
$$-\frac{\pi}{m^2}u\left\{f - v\frac{\partial m}{\partial x} + u\frac{\partial m}{\partial y}\right\} - \frac{\pi}{m}\frac{\partial \varphi}{\partial y} - C_p\frac{\pi\theta}{m}\frac{\partial P^\kappa}{\partial y} + \frac{\pi}{m^2}F_v + \frac{g}{m^2}\left(\frac{\partial \vec{\tau}}{\partial \sigma}\right)_y. \tag{3}$$

Thermodynamic Energy Equation

$$\frac{\partial}{\partial t}\left(\frac{\pi}{m^2}\theta\right) = -\frac{\partial}{\partial x}(u^* \theta) - \frac{\partial}{\partial y}(v^* \theta) - \frac{\partial}{\partial \sigma}\left(\frac{\pi}{m^2}\dot{\sigma}\theta\right)$$
$$+\frac{\pi}{m^2}F_T + \frac{\pi}{m^2}Q + \frac{g}{C_p}\frac{1}{m^2 P^\kappa}\frac{\partial H}{\partial \sigma}. \tag{4}$$

Equation for water vapour

$$\frac{\partial}{\partial t}\left(\frac{\pi}{m^2}q\right) = -\frac{\partial}{\partial x}(u^* q) - \frac{\partial}{\partial y}(v^* q) - \frac{\partial}{\partial \sigma}\left(\frac{\pi}{m^2}\dot{\sigma}q\right)$$
$$+\frac{\pi}{m^2}F_q + \frac{\pi}{m^2}M + \frac{g}{m^2}\frac{\partial E}{\partial \sigma}. \tag{5}$$

Continuity–tendency–and $\dot{\sigma}$ –equations

$$\frac{\partial}{\partial t}\left(\frac{\pi}{m^2}\right) = -\frac{\partial u^*}{\partial x} - \frac{\partial v^*}{\partial y} - \frac{\partial}{\partial \sigma}\left(\frac{\pi}{m^2}\dot{\sigma}\right), \tag{6}$$

$$\frac{\partial}{\partial t}\left(\frac{\pi}{m^2}\right) = -\int_0^1\left\{\frac{\partial u^*}{\partial x} - \frac{\partial v^*}{\partial y}\right\}d\sigma, \tag{7}$$

$$\left(\frac{\pi\dot{\sigma}}{m^2}\right)_\sigma = \left(\frac{\pi\dot{\sigma}}{m^2}\right)_{\sigma+\Delta\sigma} + \int_\sigma^{\sigma+\Delta\sigma}\left\{\frac{\partial}{\partial t}\left(\frac{\pi}{m^2}\right) + \frac{\partial u^*}{\partial x} + \frac{\partial v^*}{\partial y}\right\}d\sigma. \tag{8}$$

Hydrostatic Equation

$$\frac{\partial \varphi}{\partial \sigma} = -C_p\theta\frac{\partial P^\kappa}{\partial \sigma}. \tag{9}$$

Gas Law Equation

$$\alpha = \frac{RT}{\pi\sigma + p_T},$$

where

$$u^* = u\frac{\pi}{m}, \quad v^* = v\frac{\pi}{m}, \quad \kappa = \frac{R}{C_p}$$

and

$$P = \left(\frac{p}{1000}\right).$$

$\bar{\tau}$ is the eddy stress of momentum, F_u, F_v, F_θ and F_q are horizontal diffusion for u, v, θ and q respectively. H and E, are vertical eddy flux of heat and water vapour respectively. Q is diabatic heating (cooling) per unit mass. M is change of water vapour per unit mass. Other symbols have their usual meanings.

III. MODEL STRUCTURE AND DATA

In vertical the model has six sigma levels close to 950, 850, 700, 500, 300 and 150 hPa pressure levels. The sigma levels are 0.94, 0.83, 0.67, 0.44, 0.22 and 0.06. σ equal to 1 and 0 coincides with the bottom topography and the top of the model atmosphere (= 100 hPa) respectively. The model is staggered in the vertical. The horizontal wind components, geopotential height, temperature and mixing ratio for water vapour are defined at these sigma levels. The vertical σ –velocity ($\dot{\sigma}$) is specified at intermediate levels. The vertical structure of the model is given in Fig.1. The domain of integration extends from 10°s to 40°N and 40°E to 120°E. The horizontal grid interval used is 200 km on Mercator projection true at 23° north–south latitudes. Arakawa's B–type of staggering is used. In this type of staggered grid, the wind components are set at the centre of the grid lattice and all other parameters viz, geopotential height, temperature, mixing ratio and vertical σ–velocity are defined at corners of grid lattice. There are 41 × 29 grid points in the horizontal domain. The data of 12 GMT 4 July 1979, 12 GMT 7 July 1979 and 12 GMT 8 August 1979 extracted from FGGE IIIB data set have been used as input. The synoptic features of interest are the intense monsoon depressions on 7 July and 8 August 1979 and the formative stage of monsoon depression on 4 July 1979. The computational work of the present study was carried out on NEC–S–1000 computer system of National Informatics Centre at Pune.

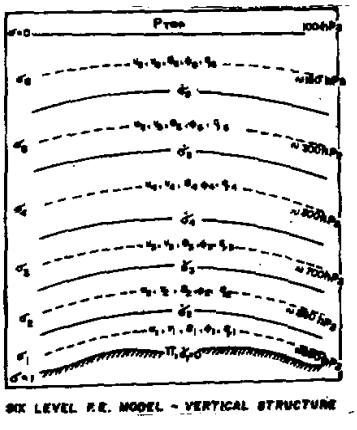

Fig.1. Vertical structure of the model.

IV. BOUNDARY CONDITIONS AND FINITE DIFFERENCE SCHEME

In vertical, the $\dot{\sigma}=0$ at $\sigma=1$ and at $\sigma=0$. In horizontal, the time invariant boundary conditions are used. All the parameters at the boundary points are kept constant throughout the period of integration.

Following Arakawa and Mintz (1974) and Arakawa and Lamb (1977) mass, energy, potential temperature and variance of potential temperature conserving finite difference scheme for space derivatives has been adopted. the horizontal advection terms in the momentum equations has been computed with fourth order accuracy difference scheme. Other terms in the equations are computed with second order accuracy scheme. Detail description of the scheme are given in Electronic Computation Centre JMA (1980). The leapfrog scheme with Asselin (1972) time filter is adopted for marching in time. The time step of 3 minutes is found suitable for the grid chosen.

V. PHYSICAL PROCESSES

The physical processes included in the model are the large scale precipitation, Kuo (1974) type cumulus convection and dry convective adjustment. Details of these processes are given by Singh (1985). The actual orography with smooth configuration is included. the effects of horizontal and vertical diffusion and surface fluxes of momentum, heat and water vapour as described in the following subsections, are also included.

1. *Subgrid Scale Horizontal Diffusion*

The diffusion is included in the model for redistribution of physical parameters by small scale eddies. The diffusion is also found effective in preventing the nonlinear computational instability.

Following are the expression for the diffusion terms based on a fourth order formulation

$$F_u = -K_H \nabla \cdot \left\{ \pi \nabla \left(\nabla_-^2 u \right) \right\} - K_{div} \pi \frac{\partial}{\partial x} \left\{ \nabla_+^2 \left(\nabla \cdot \vec{V} \right) \right\},$$

$$F_v = -K_H \nabla \cdot \left\{ \pi \nabla \left(\nabla_-^2 v \right) \right\} - K_{div} \pi \frac{\partial}{\partial y} \left\{ \nabla_+^2 \left(\nabla \cdot \vec{V} \right) \right\},$$

$$F_\theta = -K_H \nabla \cdot \left\{ \pi \nabla \left(\nabla_-^2 \theta \right) \right\},$$

$$F_q = -K_H \nabla \cdot \left\{ \pi \nabla \left(\nabla_+^2 q \right) \right\},$$

where F_u and F_v are diffusion terms for u and v momentum equations, F_θ for thermodynamic equation and F_q for water vapour equation. The momentum equation includes two diffusion terms. The first term is the same as those in the thermodynamic and water vapour equations and it acts on both rotational and divergent component of $\mathbf{V}$. The second term acts only on the divergent component of $\mathbf{V}$. The diffusion coefficients are $K_H = 5\times 10^4 \mathrm{m^2 s^{-1}}$ and $K_{d\omega} = 10^5 \mathrm{m^2 s^{-1}}$. The diffusion coefficients are constant for all grid points in the domain.

2. *Vertical Diffusion*

The exchange of momentum, heat and water vapour is taken into account as follows

$$\vec{\tau} = \frac{\rho^2 g}{\pi} K_v \frac{\partial \mathbf{V}}{\partial \sigma},$$

$$H = \frac{C_p \rho^2 g}{\pi} K_\theta \frac{\partial \theta}{\partial \sigma},$$

$$E = \frac{\rho^2 g}{\pi} K_q \frac{\partial q}{\partial \sigma},$$

where $\vec{\tau}$ is eddy stress term for momentum and H and E are the vertical turbulent fluxes of heat and moisture respectively. K_v, K_θ and K_q are the vertical eddy viscosities for momentum, heat and water vapour respectively. They are defined as

$$K_v = K_\theta = K_q = l^2 \Phi,$$

where l is mixing length and is equal to 30 meters. Φ is a function of vertical wind shear and static stability.

$$\Phi = \sqrt{\frac{\rho g}{\pi}\left\{\frac{\rho g}{\pi}\left(\frac{\partial v}{\partial \sigma}\right)^2 + \frac{g}{\theta}\frac{\partial \theta}{\partial \sigma}\right\}}.$$

The vertical exchange is applied to lower two layers of the model atmosphere.

3. *Surface Fluxes*

The surface fluxes of momentum, heat and moisture are included as follows:

$$\tau_s = \rho_s c_D |\mathbf{V}_s| \mathbf{V}_s,$$

$$H_s = \rho_s c_p c_H |\mathbf{V}_s|(T_g - T_s), \qquad T_s = \theta_s \left(\frac{p_s}{1000}\right)^\kappa$$

$$E_s = \rho_s c_E |\mathbf{V}_s|(q_g - q_s).$$

c_D, c_H and c_E are bulk coefficients for momentum, heat and water vapour respectively. The subscript s is used for the parameters related to lowest layer.

$$v_s = 0.8 v_1 \quad \text{(over sea)}; \qquad v_s = 0.69 v_1 \quad \text{(over land)}$$

$$\theta_s = \theta_1; \qquad q_s = q_1$$

Subscript g is related to values on earth's surface, T_g is monthly normal mean temperature over sea and q_g is saturated mixing ratio for the temperature T_g. The surface fluxes of heat and moisture are considered over the sea only. The formulation for bulk coefficients is based on Kondo (1975).

VI. INITIALIZATION SCHEME

The initial data for a primitive equation model needs to be in balance, otherwise during the course of time integration, the excitation of high frequency waves may lead to computational instability. Different initialization schemes have been developed and used in NWP models. The dynamic initialization and normal model initialization scheme are commonly used in research and operational NWP models. In dynamic initialization (DI) scheme, model equations are integrated forward and backward around initial time using a time integration scheme which has selective damping scheme for high frequency waves. In the normal mode initialization scheme (NMI) the solutions of the equations are split into normal modes

and the high frequency modes are removed. A new method similar to NMI has been suggested by Sugi (1986) known as dynamic normal mode initialization scheme (DNI). In this method forcing terms in model equations are separated into linear terms and nonlinear terms. The nonlinear terms are kept constant with time although they are time dependent. Due to separation of linear and nonlinear terms, solution of the equation has one part varying with time and other part remains constant with time. Thus the solution can be expressed as

$$a_j = a_{jo} + Ae^{i\omega_j t}.$$

The constant a_{jo} is the stationary part of the normal mode which is in balance with the nonlinear forcings and the $Ae^{i\omega_j t}$ is the oscillating part. With the application of forward and backward integration with a selective damping scheme, the amplitude of the oscillating part in the high frequency mode can be made very small.

Sugi (1986) examined the parformance of NMI and DNI schemes and showed that the longer period waves undergo less damping by DNI than NMI, whereas waves with pariod smaller than 6 hr undergo stronger damping by DNI.

Following Sugi, we have adopted the dynamic normal mode initialization scheme for obtaining the initial balance. The scheme is briefly presented as follows:

From the momentum and thermodynamic energy equations linear and nonlinear terms are separated as,

u–momentum equation

nonlinear terms

$$-\frac{\partial}{\partial x}(u^* u)-\frac{\partial}{\partial y}(v^* u)-\frac{\partial}{\partial \sigma}\left(\dot{\sigma}\frac{\pi}{m^2}u\right)\ \frac{\pi v}{m^2}\left\{-v\frac{\partial m}{\partial x}+u\frac{\partial m}{\partial y}\right\}$$
$$-\frac{\pi}{m}c_p\theta'\frac{\partial P^\kappa}{\partial x},$$

linear terms

$$\pi v\frac{f}{m^2}-\frac{\pi}{m}\frac{\partial \varphi}{\partial m}-c_p\frac{\pi\bar{\theta}}{m}\frac{\partial P^\kappa}{\partial x}.$$

v–momentum equation

nonlinear terms

$$-\frac{\partial}{\partial x}(u^* v)-\frac{\partial}{\partial y}(v^* v)-\frac{\partial}{\partial \sigma}\left(\dot{\sigma}\frac{\pi}{m^2}v\right)$$
$$-\frac{\pi u}{m^2}\left\{-v\frac{\partial m}{\partial x}+u\frac{\partial m}{\partial y}\right\}-\frac{\pi}{m}c_p\theta'\frac{\partial P^\kappa}{\partial y},$$

linear terms

$$-\frac{\pi}{m^2}uf-\frac{\pi}{m}\frac{\partial \varphi}{\partial y}-c_p\bar{\theta}\frac{\pi}{m}\frac{\partial P^\kappa}{\partial y}.$$

thermodynamic energy equation

nonlinear terms

$$-\frac{\partial}{\partial x}(u^* \theta')-\frac{\partial}{\partial y}(v^* \theta')-\frac{\partial}{\partial \sigma}\left(\frac{\pi}{m^2}\dot{\sigma}\theta'\right),$$

linear term

$$-\frac{\partial}{\partial\sigma}\left(\frac{\pi}{m^2}\dot{\sigma}\bar{\theta}\right),$$

where $\bar{\theta}$ is area average of potential temperature at different level and $\theta' = \theta - \bar{\theta}$.
The mixing ratio is not allowed to change during forward–backward operation. The surface pressure also remains unchanged during the initialization.

The nonlinear tendency terms are kept constant for 20 cycles of forward–backward integration of linear terms. After each 20 cycles nonlinear terms are updated. This is repeated five times. As there is no objective criteria for convergence of the scheme, 100 cycles of forward–backward integration have been found adequate to achieve the initial balance.

VII. FORECAST RESULTS

The model was integrated upto 48 hrs for two intense monsoon depressions viz. 7 July 1979 and 8 August 1979 and one formative stage of monsoon depression viz. 4 July 1979.

1. *Results of 7 July 1979*

The forecast results of 7 July and 8 August 1979 were found similar in many respects and as such results of one case i.e. 7 July 1979 are only presented.

(1) *Wind*

The initial flow fields are shown in Fig.2. The forecast and corresponding verification wind charts are shown in Fig.3. The model performance in the lower troposphere is examined with the flow patterns at 850 hPa (Fig.3a). The typical features at this level, during southwest monsoon are the monsoon depression, the cross equatorial flow and the low level jet over Arabian Sea. It may be seen from Fig.3(a) that the cyclonic circulation associated with the depression is predicted well. The easterlies to the north is found weaker and westerlies to the south of the depression is comparable. the cross equatorial flow and the circulations along the equator are predicted well. In the forecast field, a strong narrow southwesterly flow of the order of 50 knots is seen along 15°N over Arabian Sea, which extends upto Tamil Nadu coast. The wind weakens from 50 knots to 30 knots in this narrow belt. In the observed wind charts broad band of the south–westerlies is seen over Arabian sea, with average speed of 40 knots. It extends upto eastern part of Bay and wind speed reduces to 30 knots. Branch of this band is observed to the east of the depression centre.

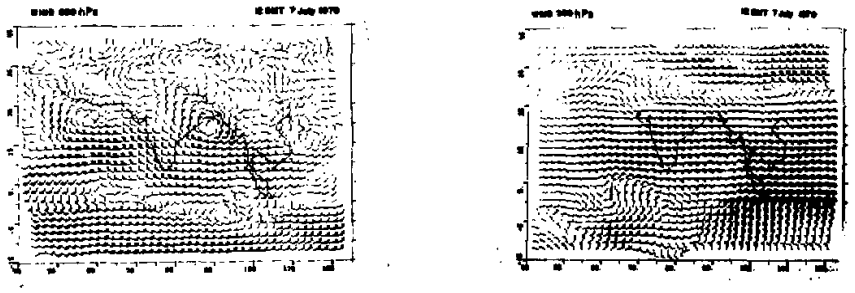

Fig.2. Initial (12 GMT 7 July 1979) wind charts at 850 hPa and 200 hPa.

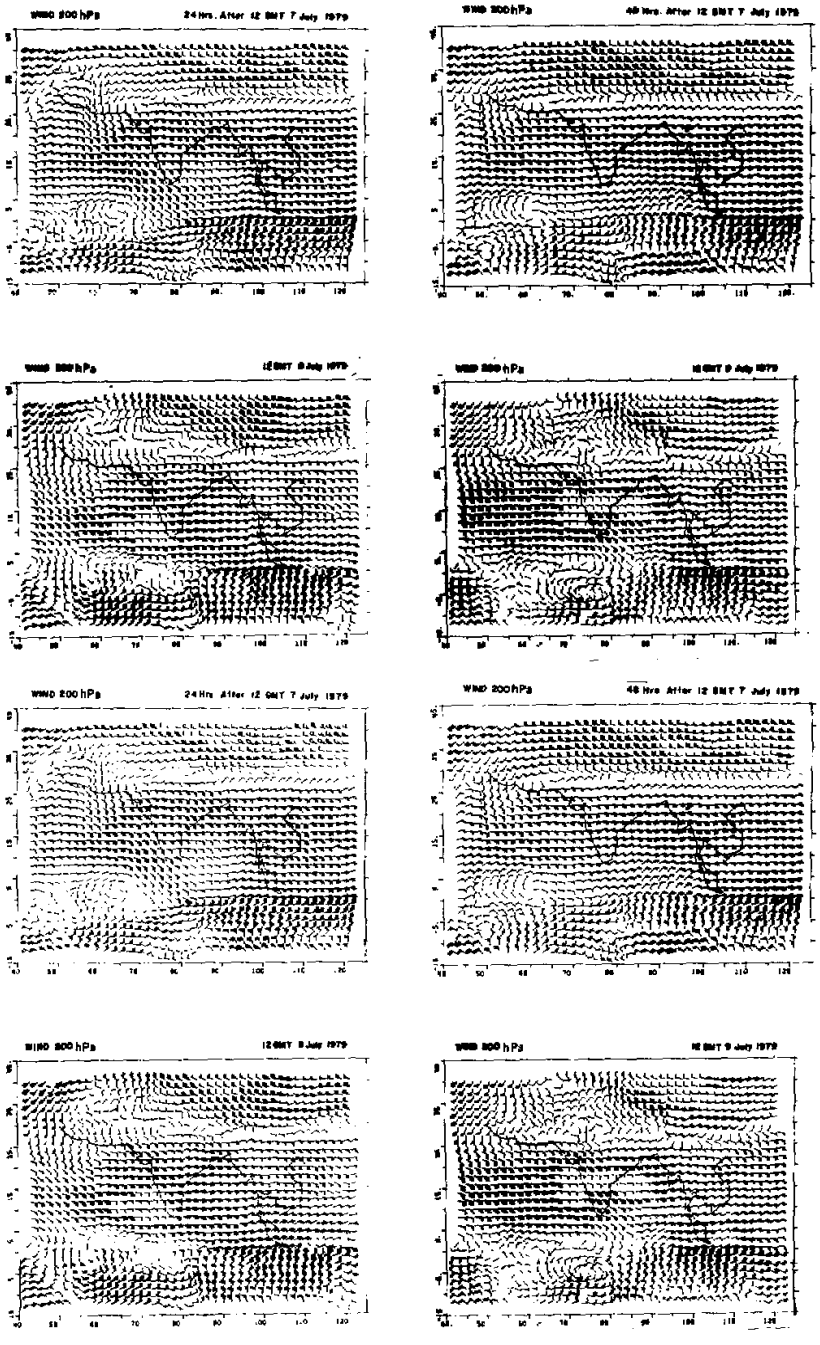

Fig.3(a). Forecast and verification wind charts at 850 hPa. (b). Same as Fig.3(a) except at 200 hPa.

To study the model performance at upper levels, 200 hPa is chosen as the representative level for the upper troposphere. Forecast and verification charts for 200 hPa are shown in Fig.3(b). During strong monsoon situations, synoptic features at upper levels are strong westerlies north of 40°N, strong easterlies along 10°N and Tibetan anticyclone over North India. In the observed charts, strong westerlies is seen north of 35°N, anticyclonic circulation is present over North India and strong easterlies is seen over Peninsular India. All these features are well predicted by the model. The strength of the westerlies is overpredicted but easterlies is underpredicted.

(2)*Track of the depression*

Track of the monsoon depression is shown in Fig.4. During first 24 hr, depression has moved north–west direction and in the next 24 hr it has moved in west–north–west direction. In the forecast during first 24 hr track of depression is similar to the observed but in the next 24 hr movement is westward instead of westnorthwest direction. The observed phase speed first 24 hr is 450 km / 24 hr and the next 24 hr it is 600 km / 24 hr. The predicted phase speed has been found comparable with those of the observed phase speed. The predicted phase speed is 330 km / 24 hr and 660 km / 24 hr in the first 24 hr and next 24 hr respectively. The vector error in the centre of depression is 150 km and 175 km in 24 hr and 48 hr forecast respectively.

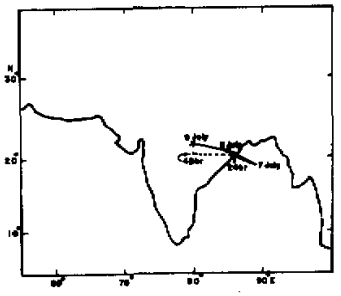

Fig.4. Track of the depression.

(3) *Vertical velocity and rainfall*

The predicted p–velocity (ω) on sigma surface is computed using following relation:

$$\omega \equiv \frac{dp}{dt} = m^2\left\{\sigma\frac{\partial}{\partial t}\left(\pi / m^2\right) + \sigma\left(\frac{u}{m}\frac{\partial \pi}{\partial x} + \frac{v}{m}\frac{\partial \pi}{\partial y}\right) + \frac{\pi\dot{\sigma}}{m^2}\right\}.$$

The verification vertical p–velocity is computed using continuity equation $\left(\frac{\partial \omega}{\partial p} + \frac{\partial u}{\partial x} + \frac{\partial v}{\partial y} = o\right)$ after adjusting the net divergence equal to zero in a vertical column.

The vertical structure of the monsoon depression is examined with the vertical cross section of vertical velocity along 22°N (Fig.5). It is seen from Fig.5 that, upward velocity associated with monsoon depression is predicted well. In 24 hr forecast a shallow cell of upward velocity is seen. Its horizontal extension is from 62°E to 90°E, whereas in observed, upward velocity extends from 72°E to 92°E and in vertical it is present upto 300 hPa. In 48 hr predicted

and observed fields, values of maximum upward velocity are comparable. The maximum upward velocity is found at 700 hPa level.

The forecast and verification fields of vertical velocity at 700 hPa are shown in Fig.6. The position and the values of the maximum upward velocity are comparable. The upward velocity is expected in southwest sector of the depression; the model is unable to predict such area of vertical velocity.

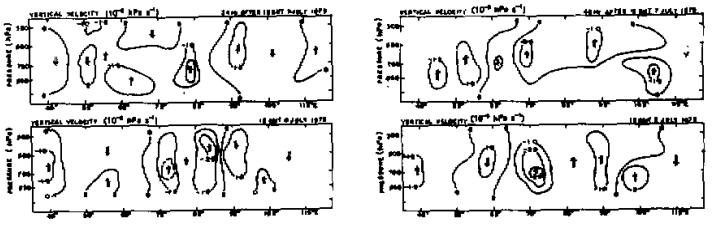

Fig.5. Vertical cross-section of forecast and observed vertical velocity along 22°N latitude (Unit: 10^{-3}hPa s^{-1}).

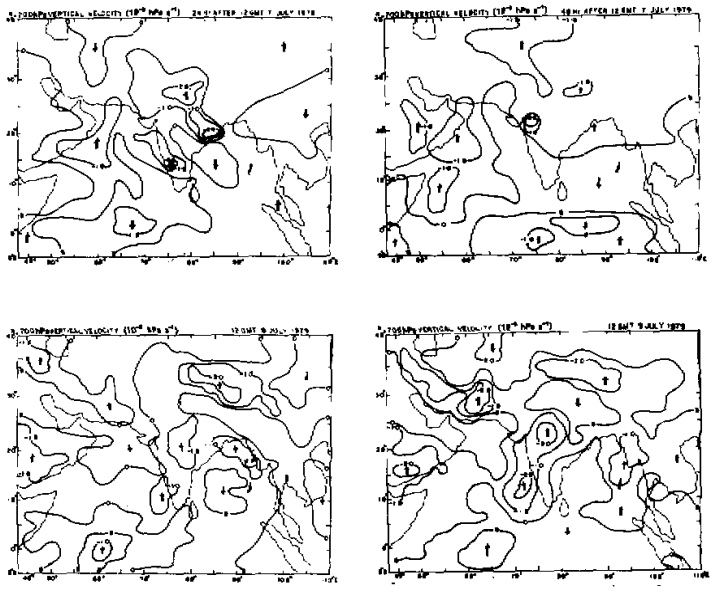

Fig.6. Forecast and corresponding verification charts of vertical velocity at 700 hPa (Unit: 10^{-3} hPa s^{-1}).

Predicted and observed rainfall rates are shown in Fig.7. For the summer MONEX, including the period of present monsoon depression, krishnamurti et al. (1983) made detailed rainfall estimates using the satellite cloud data as well as the raingauge data. These rainfall estimations are used for verification in the present study. The position of the maximum rainfall and rain area are predicted well whereas predicted rainfall rates are under-predicted.

2. *Results of 4 July 1979*

To test model's performance during the formative stage of monsoon depression, the

model has been integrated upto 48 hrs using data of 12 GMT 4 July 1979 as input. Fig.8 shows input, predicted and observed wind fields at 850 hPa. It may be seen from the 24 hr forecast wind chart that the cyclonic circulation associated with the depression has been simulated well. However, the shallowing of the cyclonic circulation could be seen in the 48 hr forecast. The cross equatorial flow is predicted satisfactorily. It may be inferred from the above results that model is able to simulate some of the features of the formative stage of monsoon depression as seen in the 24 hr forecast wind chart. However, the shallowing of the cyclonic system as seen in 48 hr wind chart is a probable indication of the beginning of damping beyond 24 hrs integration. The observed and predicted rainfall rates are shown in Fig.9. The rainfall area associated with the system is predicted well but rainfall rates are under–predicted. the observed maximum rainfall is 140 mm / 24 hr whereas predicted rainfall rate is 70 mm / 24 hr.

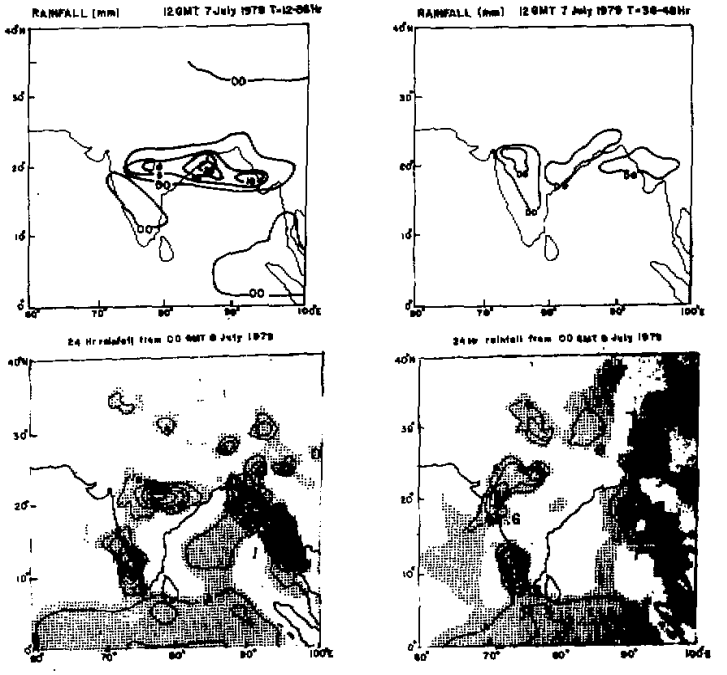

Fig.7. Predicted and observed (Krishnamurti et al. 1983) 24 hr rainfall (mm). The predicted rainfall for the period from 00 GMT 9 July (top right panel) is 12 hour rainfall.

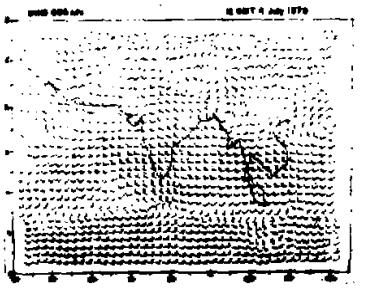

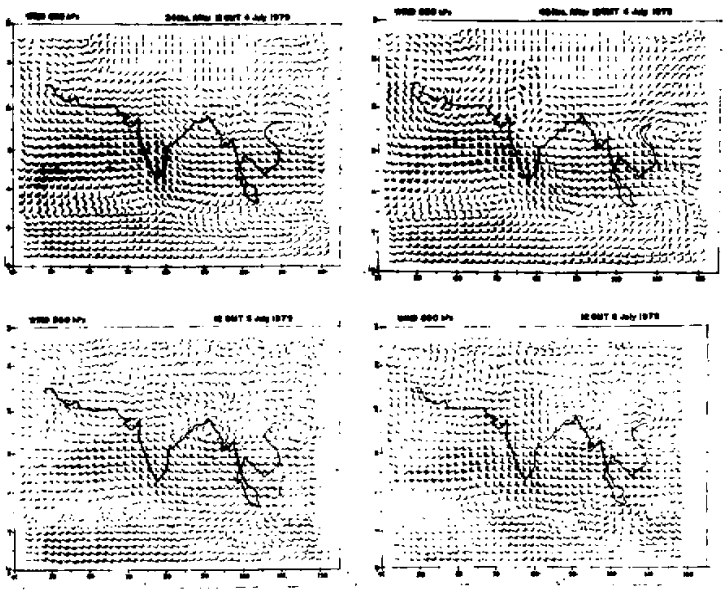

Fig.8(a). Initial (12 GMT 4 July 1979) wind chart at 850 hPa. (b). Forecast and verification wind charts at 850 hPa.

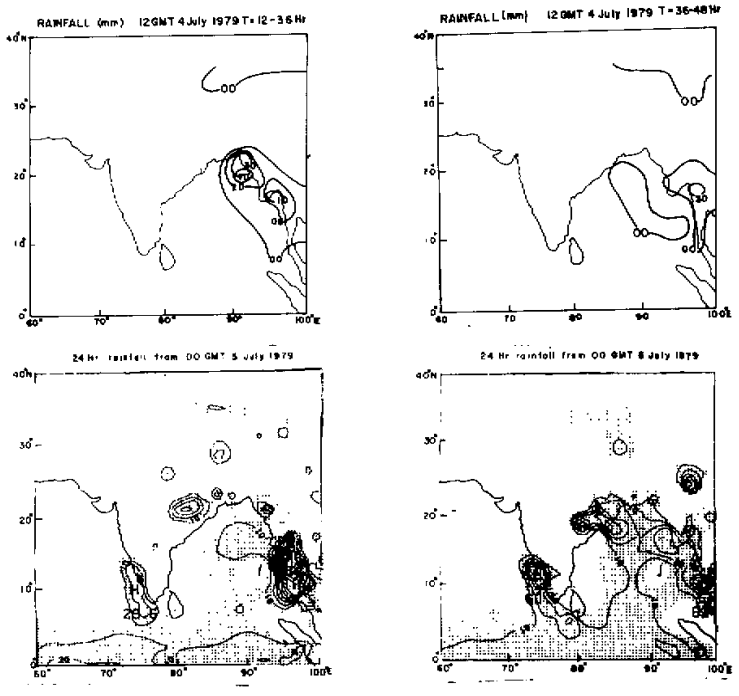

Fig.9. Same as Fig.7 but for 12 GMT July 1979 input.

VIII. ENVELOPE OROGRAPHY

1. *Concept of Envelope Orography*

Wallace et al. (1983) introduced the notion of envelope orography in ECMWF grid point numerical weather prediction model following Messinger (1977) and Bleck (1977). Mesinger and Bleck suggested that mesoscale circulations might be parameterized in large–scale numerical weather prediction models by treating the sheltered basins and mountain valleys as though they were part of the terrain itself. Wallace et al. created envelope orography simply by adding, before the final smoothing operation, to the grid–point mean orography an additional increment equal to a constant times the sub–grid–scale standard deviation of the high resolution orography about its grid–point mean value. They found that a constant of 2.0 would yield a true envelope orography whose height is equal to that of the mountain tops. Such a representation of orography appears to be most effective for rough mountain ranges, which is considerably under–represented in the conventional smoothed orography, The envelope orography not only increases the maximum height of the mountain ranges, but it also results in a substantial increase in the area covered by high terrain. Using ECMWF model, Wallace et al. further showed that the envelope orography is capable of yielding more realistic simulation of the observed wintertime flow. The high resolution orography data used by them to construct the envelope orography was taken from the US Navy data set which has a resolution of $1/6^{\circ}$ latitude $\times 1/6^{\circ}$ longitude.

Krishnamurti et al. (1984) explored the sensitivity of monsoon circulations to normal and envelope orography using a global spectral model. Their experiments with envelope orography showed a major improvement in the monsoon region. They found that with the steeper Western Ghats track of the monsoon onset vortex is predicted extremely well, while with the normal orography the vortex tends to move far inland. They also noted that the envelope orography has an adverse effect on the divergent winds east of the Himalayas over western China and around the Andes.

In the present study we propose to investigate the impact of envelope orography on monsoon prediction using the regional model described in the previous sections.

2. *Experiments with Envelope Orography*

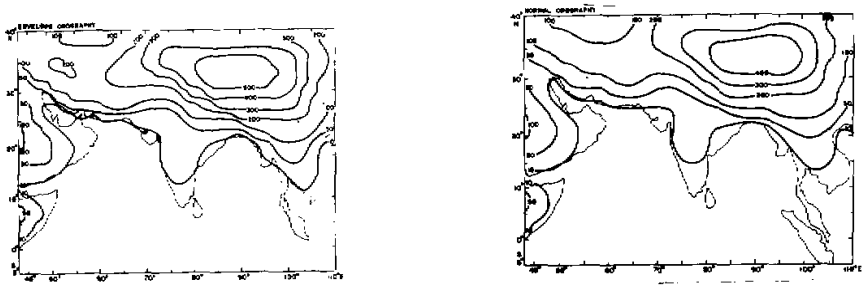

Fig.10. Normal and Envelope orography (Unit: decameter).

We carried out prediction experiments with envelope and normal orography using adiabatic version of the model. In each experiment the model was integrated upto 48 hrs using input of 7 July 1979. The envelope orography was created following Wallace et al. (1983) with the 1° latitude $\times 1^{\circ}$ longitude Scrips topography data. The envelope orography increased

the horizontal extent of the area covered by the mountains and height of the highest mountains are increased by about 1 km (Fig.10). Due to the coarse resolution of 1° latitude x 1° longitude used to construct the envelope orography, we find that the narrow orographic barriers like Western Ghats and Burmese mountains are not adequately represented. It is understandable that the realistic envelope orography can not be constructed with such coarse orographic data. Our objective in the present study is to make an attempt towards understanding the impact of envelope orography on the monsoon prediction and also to what extent the orography gets modified.

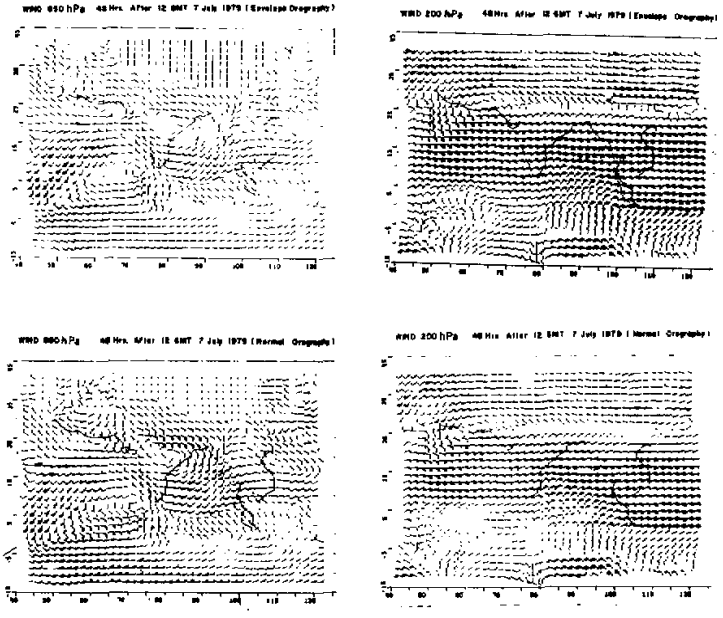

Fig.11. 48 hr forecast wind charts at 850 hPa and 200 hPa with envelope and normal orography.

48 hr forecast wind charts are shown in Fig.11. The corresponding verification wind charts are given in Fig.3 (a–b). Evaluation of the forecast results show that the circulation features are predicted quite well with envelope and normal orography. In the 24 hr forecast (not presented) the predicted wind around the monsoon depression is weaker than the actual in both experiments. The 48 hr winds around the depression are comparable to the actual. The 24 hr forecast of the depression centre with envelope orography is at 21°N, 84°E, while it is at 21.5°N, 86°E with normal orography. The 48 hr forecast centre is at 19°N, 82°E for the envelope orography and 21°N, 81°E for the normal orography. The depression centre is at 21°N, 85°E on 8 July 1979 and 22°N, 80°E on 9 July 1979. In general predicted track of the depression is south of the observed track. Furthermore, the predicted centre of depression with envelope orography is more considerably shifted towards south than that observed in case of normal orography. The southward shift of the depression centre in the experiment with envelope orography could be due to the southward extension of Himalayan mountains. In both the experiments the upper tropospheric core of strong westerlies in the higher latitudes are overpredicted and the core of easterlies in the lower latitudes is under–predicted.

We have also run the diabatic version of the model with envelope orography and com-

pared the precipitation rates and phase speed of the monsoon depression obtained with normal orography. We found little change in the precipitation rates and phase speed. The possible reason for little change in rainfall and phase speed could be due to the underrepresentation of the Western Ghats and Burmese mountains in the envelope orography.

IX. CONCLUDING REMARKS

A six level primitive equation model in sigma coordinate has been formulated and applied for monsoon prediction. The model has been integrated upto 48 hrs. The flow patterns, cross–equatorial flow and structure of the depression are predicted satisfactorily, but the movement is found slower than the actual. The rainfall region is also predicted reasonably well, however, the precipitation rates are underpredicted. The movement of the monsoon depression is normally attributed to the convergence produced in the forward sector due to release of latent heat. Since the rainfall rates produced by the model is much lower than the actual, this implies that the convergence is also weaker than the actual in the forward sector, thereby slowing down the forecast movement of the cyclonic circulation.

It was pointed out by Singh et al. (1988) that for a realistic monsoon rainfall prediction, the divergent wind should be modified over the rainfall region through physical initialization (Krishnamurti et al., 1984), so that the cumulus parameterization of the model (Kuo Scheme) can reproduce the observed rainfall rates as much as possible at the initial time. The formulation and testing for the modification of divergent wind using observed precipitation rates for the model is being done and the results will be reported later. The other factors influencing poor prediction of rainfall rates could be (i) the complete absence of heat and moisture supply from the land surface and (ii) the error involved in the computation of heat and moisture supply from the sea surface by using mean monthly sea surface temperature, which might deviate significantly from the sea surface temperature of the input day.

In order to provide effective treatment to the steepness in topography, the envelope orography was constructed and included in the model. The results did not show improvement in the forecast. This is quite understandable as the envelope orography was constructed using coarse grid of 1° latitude–longitude grid.

Despite a few shortcomings outlined above, the model with necessary physical processes and realistic topography could be effectively utilized for studies on different initialization schemes, lateral boundary conditions including nested grid, parameterization of cumulus convection, boundary layer parameterization and in the treatment of orography.

The authors would like to thank Shri D. R. Sikka, Director, Indian Institute of Tropical Meteorology, Pune for his interest in the study. Thanks are also due to Drs. S. K. Mishra and P. S. Salvekar for going through the manuscript and giving valuable comments. Their thanks are due to Smt. C. Bardhan for typing the manuscript and to Shri R. M. Soni for drafting the diagrams.

REFERENCES

Arakawa, A. and Lamb, V.R., (1977) Computational design of the basic dynamical processes of the UCLA general circulation model, *Methods Compu. Physics*, **17**: 173–265.

Arakawa, A. and Mintz, Y., (1974), The UCLA Atmospheric General Circulation model (with the participation of A. katayama, J.W. Kim, W. Schubert, T. Topkioka, M. Schlesinger, W. Chao, D. Randall and L. lord) Notes distributed at the Workshop, 25 March–4 April, 1974, Department of Meteorology, University of California.

Asselin, R., (1972), Frequency filter for time integration, *Mon. Wea. Rev.* **100**: 487–490.

Bleck, R., (1977), Numerical simulation of lee cyclogenesis in the Gulf of Genoa, *Mon. Wea. Rev.*, **105:** 428–445.

Electronic Computation Centre JMA, (1980), Outline of operational numerical weather prediction at Japan Meteorological Agency, Appendix to Periodic Report on Numerical Weather Prediction, 23–36.

Electronic Computation Centre JMA, (1983), Outline of operational numerical weather prediction at Japan Meteorological Agency, Appendix to Periodic Report on Numerical Weather Prediction, 33–48.

Kondo, J., (1975), Air–sea bulk transfer coefficients in diabatic conditions, *Bound. Layer. Meteor.*, **9:** 91–112.

Krishnamurti, T.N., Steven Cocke, Richard Pasch, Simon Low–Nam, (1983), Precipitation estimates from rain-gauge and satellite observations summer MONEX.

Krishnamurti, T. N., Ingles, K., Cocke, S., Kitade, T., and Pasch, R., (1984), Details of low latitude medium range numerical weather prediction using a global spectral model Part II. Effects of orography and physical initialization, **62:** 613–648.

Kuo, H. L., (1974), Further studies of the parameterization of the influence of cumulus convection on large scale flow, *J.Atm.Sci.*, **31:** 1232–1240.

Mesinger, F., (1977), Forward–Backward Scheme and its use in a limited–area model, *Beitr. Zur. Phys. der Atmos.*, **50:** 200–210.

Singh, S. S., (1985), Short range prediction with a multilevel primitive equation model, *Proc. Indian Acad. Sci.* (Earth and Planet. Sci.), **94:** 159–184.

Singh, S. S., Bandyopadhyay, A. and Vaidya, S. S., (1988), Impact of convective transfer of heat and moisture on prediction of monsoon depression, Mausam, **39:** 19–26.

Sugi, M., (1986), Dynamic normal mode initialization, *J. Met. Soc. Japan*, **64:** 623–636.

Wallace, J. M., Tibaldi, S. and Simmons, A.J. (1983), Reduction of systematic forecast errors in the ECMWF model through the introduction of an envelope orography, *Quart. J. R. Met. Soc.*, **109:** 683–717.